Study of the Directivity of Parametric Arrays

Karsten Wiedmann, Tobias Weber
Institute of Communications Engineering, University of Rostock
Richard-Wagner-Str. 31, 18119 Rostock, Germany
Email: {karsten.wiedmann}{tobias.weber}@uni-rostock.de

Introduction

In parametric underwater communications (PUC) [1, 2, 3, 4], nonlinear effects occurring during the propagation of intense acoustic waves are exploited for communication purposes. For this, a high-frequency wave, called primary wave, is radiated by a transducer. Due to intermodulation of this primary wave, among others new low frequency components are generated. This nonlinearly generated wave is denoted as secondary wave. Using appropriate modulation techniques [1], the information of the primary wave can be recovered from the secondary wave. Besides the reduced channel attenuation at low-frequencies, the secondary wave features a high relative bandwidth and a high directivity so that this approach is promising for communication purposes in long-range acoustic underwater channels.

Theoretical investigations in order to assess the capabilities of PUC are challenging owing to the underlying nonlinear acoustics. In particular, investigations of the secondary directivity of PUC systems are usually done by means of numerical simulations. The simulations are convenient and match with real-world measurements fairly well. But this way, only limited physical insights into the directivity causing processes can be gathered. Analytical investigations are more suitable for this purpose. Here, a key problem is in the modelling of the primary wave propagation in connection with the nonlinear wave generation. Corresponding analytical approaches imply a volume integration over the virtual source strength density and closed form solutions suffer from simplifying assumptions or can only be partially derived.

This paper shows that using a spherical harmonics expansion for the primary wave can simplify the study of the secondary directivity. Along with the quasi-linear approach [5], the virtual volume source is separated in a transversal and a radial dependent component. Then, the volume integration can be accordingly separated by employing Green's function in spherical harmonics. The integration over the transversal dependent component simplifies significantly due to the orthogonality of the spherical harmonics. More importantly, it is not explicitly required to carry out the integration over the radial dependent component for an analysis of the directivity. This enables the derivation of closed form solutions for elementary primary sources and an investigation of the directional effects in parametric arrays.

Using the discussed approach, it is analytically shown for an arbitrary primary source that the secondary directivity pattern approaches the squared primary directivity pattern, if the secondary wave is mainly generated in the primary farfield. If contrarily the secondary wave is generated in both the primary nearfield and farfield, a broadening of the secondary directivity pattern is observed. This is in agreement with the literature [2]. As an example, the directivity of a primary dipole source is discussed in the paper.

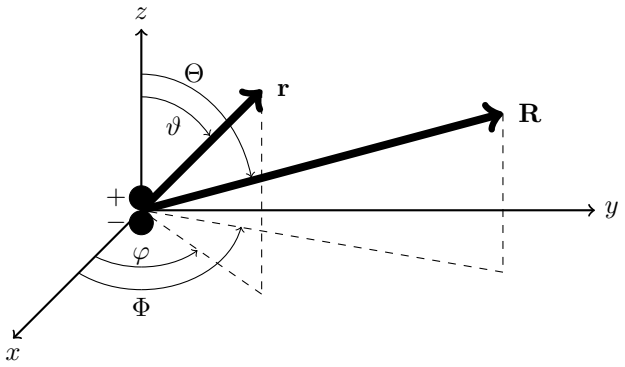

Fig. 1: Considered geometry with a primary z-axial dipol source in the origin.

Physical Modelling

A physical source being located at the origin of a spherical coordinate system, see Fig. 1, with r denoting the radial distance, ϑ the polar angle and φ the azimuthal angle of a point $\mathbf{r} = [r, \vartheta, \varphi]^{\mathrm{T}}$ is considered. The physical source radiates a primary wave, which is denoted by its sound pressure $\underline{P}_{\mathrm{p}}(\mathbf{r}, \omega)$ in the spectral domain. Due to the low conversion efficiency of the nonlinear wave generation process, it is assumed that only intermodulation in the primary wave needs to be considered and that the primary wave propagates mainly in a linear manner. Following this so-called quasi-linear approach [5], the primary wave $\underline{P}_{\mathrm{p}}(\mathbf{r}, \omega)$ satisfies the linear Helmholtz equation [6]. For simplicity, a two-tone excitation with the frequencies ω_1 and ω_2 is considered in this paper. With k_1 and k_2 denoting the corresponding wave numbers and $\underline{\tilde{P}}_{\mathrm{p}}(\mathbf{r},k)$ denoting the complex amplitudes, the primary wave reads

$$\begin{aligned}\underline{P}_{\mathrm{p}}(\mathbf{r}, \omega) = \underline{\tilde{P}}^{*}_{\mathrm{p}}(\mathbf{r},k_1)\delta(\omega + \omega_1) + \underline{\tilde{P}}_{\mathrm{p}}(\mathbf{r},k_1)\delta(\omega - \omega_1) \\ + \underline{\tilde{P}}^{*}_{\mathrm{p}}(\mathbf{r},k_2)\delta(\omega + \omega_2) + \underline{\tilde{P}}_{\mathrm{p}}(\mathbf{r},k_2)\delta(\omega - \omega_2)\ . \quad (1)\end{aligned}$$

Using spherical coordinates and applying a separation of variables [6], the complex amplitudes $\underline{\tilde{P}}_{\mathrm{p}}(\mathbf{r},k)$ satisfying the homogeneous Helmholtz equation can be written in

the form

$$\underline{\tilde{P}}_{\mathrm{p}}(\mathbf{r},k) = e^{-\alpha r} \sum_{a=0}^{\infty} \sum_{b=-a}^{a} \underline{A}_{a,b} \underline{h}_a(kr) \underline{Y}_a^b(\vartheta,\varphi) \ , \qquad (2)$$

where $\underline{A}_{a,b}$ are complex coefficients, $\underline{h}_a(kr)$ are the spherical Hankel functions of first kind for an outgoing wave and $\underline{Y}_a^b(\vartheta,\varphi)$ are the spherical harmonics [6]. With α denoting an attenuation coefficient, attenuation due to absorption is considered for the primary wave $\underline{\tilde{P}}_{\mathrm{p}}(\mathbf{r},k)$ in (2).

Nonlinear effects take place at every point $\mathbf{r}$ where the primary waves are intense so that a secondary wave is radiated by a virtual source volume. At a point $\mathbf{R} = [R, \Theta, \Phi]^{\mathrm{T}}$, the secondary wave $\underline{P}_{\mathrm{s}}(\mathbf{R},\omega)$ satisfies the inhomogeneous wave equation [6]

$$k^2 \, \underline{P}_{\mathrm{s}}(\mathbf{R},\omega) + \Delta \underline{P}_{\mathrm{s}}(\mathbf{R},\omega) = \underline{Q}(\omega) \ , \qquad (3)$$

with $\underline{Q}(\omega)$ denoting the (virtual) source strength density. It can be shown in the time-domain by means of a physical modelling [1, 5, 7] that the virtual source strength density is proportional to the squared primary wave. Transformed into the frequency domain, the source strength density $\underline{Q}(\mathbf{r},\omega)$ at a point $\mathbf{r}$ is obtained by auto-convolving the primary wave $\underline{P}_{\mathrm{p}}(\mathbf{r},\omega)$ at $\mathbf{r}$ with respect to the frequency ω and a subsequent weighting by ω^2 and a constant β, reading

$$\underline{Q}(\mathbf{r},\omega) = \beta k^2 \left(\underline{P}_{\mathrm{p}}(\mathbf{r},\omega) *_{\omega} \underline{P}_{\mathrm{p}}(\mathbf{r},\omega) \right) \ . \qquad (4)$$

Since only the low frequency components are of interest for PUC, from the auto-convolution of (4) only the terms with the difference frequency $\omega_{\mathrm{d}} = \omega_1 - \omega_2$ are considered in the following. Substituting the primary wave (1) in the source strength density (4) and considering only terms at ω_{d}, it follows

$$\begin{aligned} \underline{Q}_{\mathrm{d}}(\mathbf{r},\omega) = {} & \beta k_{\mathrm{d}}^2 \, \underline{\tilde{P}}_{\mathrm{p}}(\mathbf{r},k_1) \underline{\tilde{P}}_{\mathrm{p}}^*(\mathbf{r},k_2) \delta(\omega + \omega_{\mathrm{d}}) \\ & + \underbrace{\beta k_{\mathrm{d}}^2 \, \underline{\tilde{P}}_{\mathrm{p}}^*(\mathbf{r},k_1) \underline{\tilde{P}}_{\mathrm{p}}(\mathbf{r},k_2)}_{\underline{\tilde{Q}}(\mathbf{r},k_{\mathrm{d}})} \delta(\omega - \omega_{\mathrm{d}}) \ , \end{aligned} \qquad (5)$$

where $\underline{\tilde{Q}}_{\mathrm{d}}(\mathbf{r},k_{\mathrm{d}})$ denotes the complex amplitude of the source strength density for the difference frequency. Next, a spherical harmonics expansion of the complex amplitude $\underline{\tilde{Q}}_{\mathrm{d}}(\mathbf{r},k_{\mathrm{d}})$ in (5) is considered. With the complex coefficients $\underline{B}_{m,n}$ together with the substitution of (2) into (5), it follows for the complex amplitude

$$\begin{aligned} \underline{\tilde{Q}}_{\mathrm{d}}(\mathbf{r},k_{\mathrm{d}}) &= e^{-2\alpha r} \sum_{n=0}^{\infty} \sum_{m=-n}^{n} \underline{B}_{m,n} \underline{h}_n(k_{\mathrm{d}} r) \underline{Y}_n^m(\vartheta,\varphi) \\ &\overset{!}{=} \beta k_{\mathrm{d}}^2 e^{-2\alpha r} \sum_{a,c=0}^{\infty} \sum_{b=-a}^{a} \sum_{d=-c}^{c} \underline{A}_{a,b}^* \underline{A}_{c,d} \underline{h}_a^*(\cdot) \underline{h}_c(\cdot) \underline{Y}_a^{b*}(\cdot) \underline{Y}_c^d(\cdot). \end{aligned} \qquad (6)$$

Since the spherical harmonics $\underline{Y}(\vartheta,\varphi)$ are basis functions, the corresponding products in (6) can be expressed as linear combinations of the basis functions, i.e.,

$$\underline{Y}_a^{b*}(\vartheta,\varphi) \underline{Y}_c^d(\vartheta,\varphi) = \sum_{v=|a-c|}^{a+c} \sum_{w=-v}^{v} \kappa_{v,w} \underline{Y}_w^v(\vartheta,\varphi) \ , \qquad (7)$$

where the coefficients $\kappa_{v,w}$ can be determined by means of the Clebsch–Gordan coefficients [8]. Using (7), the coefficients $\underline{B}_{m,n}$ in (6) can be expressed as

$$\begin{aligned} \underline{B}_{m,n} = \beta k_{\mathrm{d}}^2 \kappa_{n,m} \sum_{a,c=0}^{\infty} \sum_{b=-a}^{a} \sum_{d=-c}^{c} \Bigg(& \underline{A}_{a,b}^* \underline{A}_{c,d} \\ & \cdot \frac{\int e^{-2\alpha r} \underline{h}_a^*(k_1 r) \underline{h}_c(k_2 r) \underline{h}_n^*(k_{\mathrm{d}} r) r^2 \mathrm{d}r}{\int e^{-2\alpha r} \underline{h}_n(k_{\mathrm{d}} r) \underline{h}_n^*(k_{\mathrm{d}} r) r^2 \mathrm{d}r} \Bigg) . \end{aligned} \qquad (8)$$

Using the equations (6)-(8) and the spherical harmonics expansion of the Green's function [6]

$$\underline{G}(\mathbf{R},\mathbf{r}) = \mathrm{j} k_{\mathrm{d}} \sum_{v=0}^{\infty} \sum_{w=-v}^{v} \underline{h}_v(k_{\mathrm{d}} R) \underline{Y}_v^w(\Theta,\Phi) j_v(k_{\mathrm{d}} r) \underline{Y}_v^{w*}(\vartheta,\varphi), \qquad (9)$$

with $j_v(k_{\mathrm{d}} r)$ denoting the spherical Bessel functions of the first kind [8], the solution for the complex amplitude of the difference frequency can be written as

$$\underline{\tilde{P}}_{\mathrm{s}}(\mathbf{R},k_{\mathrm{d}}) = - \int_{\partial V} \underline{\tilde{Q}}_{\mathrm{d}}(\mathbf{r},k_{\mathrm{d}}) \underline{G}(\mathbf{R},\mathbf{r}) \mathrm{d}\mathbf{r} \ . \qquad (10)$$

It is worth knowing that the terms of (6) and (9) are separable in radial and transversal dependent components. Thus, the volume integral in (10) can be separated in a radial and transversal dependent component, see equation (12). Using the orthogonality property of the spherical harmonics, i.e.,

$$\int_{\partial V} \underline{Y}_n^m(\vartheta,\varphi) \underline{Y}_v^{w*}(\vartheta,\varphi) \mathrm{d}A = \delta_{nv} \delta_{mw} \ , \qquad (11)$$

the volume integral of (10) reduces to an one-dimensional integral with respect to the radial dependent component.

Secondary Directivity

Equation (12) can be employed for analysing the directivity of the secondary wave. For this, the secondary wave is evaluated at the limit $R \to \infty$, enabling the large argument approximation of the spherical Hankel functions [6]

$$\lim_{R \to \infty} \underline{h}_n^{(1)}(k_{\mathrm{d}} R) \approx (-\mathrm{j})^{n+1} \frac{e^{\mathrm{j} k_{\mathrm{d}} R}}{k_{\mathrm{d}} R} \qquad (13)$$

in (12). Considering only the transversal dependent factor $\underline{D}_{\mathrm{s}}(\Theta,\Phi)$ of the result, it follows

$$\begin{aligned} \underline{D}_{\mathrm{s}}(\Theta,\Phi) = \sum_{n=0}^{\infty} \sum_{m=-n}^{n} \Bigg(& (-\mathrm{j})^{n+1} \underline{B}_{n,m} \underline{Y}_n^m(\Theta,\Phi) \\ & \cdot \int_r e^{-2\alpha r} \underline{h}_n(k_{\mathrm{d}} r) j_n(k_{\mathrm{d}} r) r^2 \mathrm{d}r \Bigg) . \end{aligned} \qquad (14)$$

Determining the absolute value of (14) and normalizing the result yields the directivity pattern of the secondary wave. This way, the secondary directivity caused by an arbitrary source strength density can be obtained from (14) by calculating the coefficients $\underline{B}_{n,m}$ resulting from

$$\underline{\tilde{P}}_{\mathrm{s}}(\mathbf{R},k_{\mathrm{d}}) = \mathrm{j}k_{\mathrm{d}} \sum_{v=0}^{\infty}\sum_{w=-v}^{v} \underline{h}_v(k_{\mathrm{d}}R)\underline{Y}_v^w(\Theta,\Phi) \sum_{n=0}^{\infty}\sum_{m=-n}^{n} \underline{B}_{n,m} \int_r e^{-2\alpha r}\underline{h}_n(k_{\mathrm{d}}r)j_v(k_{\mathrm{d}}r)r^2\mathrm{d}r \underbrace{\int_{\partial V} \underline{Y}_n^m(\vartheta,\varphi)\underline{Y}_v^{w*}(\vartheta,\varphi)\mathrm{d}A}_{\delta_{nv}\delta_{mw}}$$

$$= \mathrm{j}k_{\mathrm{d}} \sum_{n=0}^{\infty}\sum_{m=-n}^{n} \underline{B}_{n,m}\underline{h}_n(k_{\mathrm{d}}R)\underline{Y}_n^m(\Theta,\Phi) \int_r e^{-2\alpha r}\underline{h}_n(k_{\mathrm{d}}r)j_n(k_{\mathrm{d}}r)r^2\mathrm{d}r \tag{12}$$

the coefficients $\underline{A}$ of the primary wave using (8). Depending on the scenario, closed form solutions for the integral of (14) may be found in textbooks, e.g. [8].

An assessment of the secondary directivity pattern without explicitly solving the integral can be done, if the secondary wave is mainly created by the primary farfield. Since the product $k_{\mathrm{d}}r$ becomes large in the primary farfield, the large argument approximation of the Hankel function $\underline{h}_m(k_{\mathrm{d}}r)$ according to (13) can be substituted into (14) together with the large argument approximation of the spherical Bessel functions [8]

$$\lim_{r\to\infty} j_n(k_{\mathrm{d}}r) \approx \frac{1}{k_{\mathrm{d}}r}\sin\Big(k_{\mathrm{d}}r - \frac{n}{2}\pi\Big) \ . \tag{15}$$

Then, after some manipulations it follows the transversal dependence of the secondary wave

$$\underline{D}_{\mathrm{s}}(\Theta,\Phi) \sim \sum_{n=0}^{\infty}\sum_{m=0}^{\infty} (-\mathrm{j})^{2n+2}\underline{B}_{n,m}\underline{Y}_n^m(\Theta,\Phi) \cdot \left(e^{\frac{n\pi}{2}}\int_r e^{-2\alpha r}\,\mathrm{d}r - e^{-\frac{n\pi}{2}}\int_r e^{-2\alpha r+\mathrm{j}2k_{\mathrm{d}}r}\mathrm{d}r \right) . \tag{16}$$

For low attenuation coefficients α, the first integral in (16) dominates over the second one so that the latter is neglected in the following. Then, with

$$e^{\mathrm{j}\frac{n\pi}{2}}(-j)^{2n+2} = -(-\mathrm{j})^n \ , \tag{17}$$

it follows for the transversal dependence

$$\underline{D}_{\mathrm{s}}(\Theta,\Phi) \sim \sum_{n=0}^{\infty}\sum_{m=-n}^{n} (-\mathrm{j})^n\underline{B}_{n,m}\underline{Y}_n^m(\Theta,\Phi) \ . \tag{18}$$

The significance of equation (18) is clarified if the virtual source strength density (6) is evaluated at the limit $r\to\infty$. It follows the transversal dependence of the source strength density

$$\underline{D}_{\mathrm{Q}}(\vartheta,\varphi) \sim \sum_{n=0}^{\infty}\sum_{m=-n}^{n} (-\mathrm{j})^n\underline{B}_{n,m}\underline{Y}_n^m(\vartheta,\varphi) \ . \tag{19}$$

Equations (18) and (19) yield the same transversal dependencies. As a result, the directivity pattern of the secondary wave approaches the directivity pattern of the source strength density, if only the primary farfield contributes to the secondary wave.

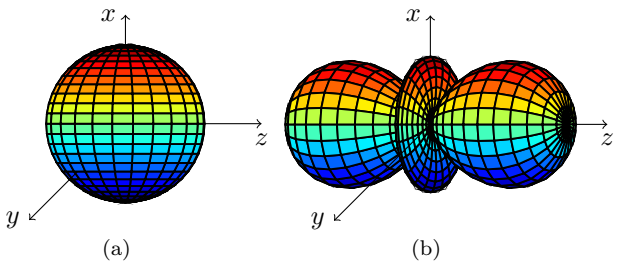

Fig. 2: Spherical harmonics: $\underline{Y}_0^0(\vartheta,\varphi)$ (a) and $\underline{Y}_2^0(\vartheta,\varphi)$ (b).

Example: Primary z-Axial Dipole Source

In the following, a z-axial dipole source [6] in the origin is considered as the primary source, see Fig. 1. The primary wave being radiated by the dipole has the complex amplitude

$$\underline{\tilde{P}}_{\mathrm{p}}(\mathbf{r},k) = \underline{A}_{1,0}e^{-\alpha r}\underline{h}_1(kr)\underline{Y}_1^0(\vartheta,\varphi) \ . \tag{20}$$

According to (6), the source strength density has the complex amplitude

$$\underline{\tilde{Q}}_{\mathrm{d}}(\mathbf{r},k_{\mathrm{d}}) = \beta k_{\mathrm{d}}^2\, e^{-2\alpha r}\left|\underline{A}_{1,0}\right|^2 \underline{Y}_1^0(\vartheta,\varphi)^2\, \underline{h}_1^*(k_1r)\underline{h}_1(k_2r) \stackrel{!}{=} \sum_{n=0}^{\infty}\sum_{m=-n}^{n} \underline{B}_{n,m}e^{-2\alpha r}\underline{h}_n(k_{\mathrm{d}}r)\underline{Y}_n^0(\vartheta,\varphi) \, . \tag{21}$$

Using (7), one obtains for the product $\underline{Y}_1^0(\vartheta,\varphi)\underline{Y}_1^0(\vartheta,\varphi)$ the coefficients

$$\kappa_{n,m} = \begin{cases} 1/\sqrt{4\pi} & n=0, m=0 \\ 1/\sqrt{5\pi} & n=2, m=0 \\ 0 & \text{else} \ . \end{cases} \tag{22}$$

Consequently, only the coefficients $\underline{B}_{0,0}$ and $\underline{B}_{2,0}$ are nonzero in (21) and only the spherical harmonics $\underline{Y}_0^0(\vartheta,\varphi)$ and $\underline{Y}_2^0(\vartheta,\varphi)$, see Fig. 2, contribute to the directivity of the secondary wave. Having said this, the transversal dependence according to (14) of the secondary wave reads

$$\underline{D}_{\mathrm{D}}(\Theta,\Phi) \sim \underline{B}_{0,0}\underline{Y}_0^0(\Theta,\Phi)\int_r e^{-2\alpha r}\underline{h}_0(k_{\mathrm{d}}r)j_0(k_{\mathrm{d}}r)r^2\mathrm{d}r - \underline{B}_{2,0}\underline{Y}_2^0(\Theta,\Phi)\int_r e^{-2\alpha r}\underline{h}_2(k_{\mathrm{d}}r)j_2(k_{\mathrm{d}}r)r^2\mathrm{d}r \tag{23}$$

with the coefficients

$$\underline{B}_{n,0} = \beta k_{\mathrm{d}}^2\kappa_{n,0}\left|\underline{A}_{1,0}\right|^2 \frac{\int e^{-2\alpha r}\underline{h}_1^*(k_1r)\underline{h}_1(k_2r)\underline{h}_n^*(k_{\mathrm{d}}r)r^2\mathrm{d}r}{\int e^{-2\alpha r}\underline{h}_n(k_{\mathrm{d}}r)\underline{h}_n^*(k_{\mathrm{d}}r)r^2\mathrm{d}r} . \tag{24}$$

Assuming for the time being that the secondary wave is mainly generated by the primary farfield, the large-argument approximations of (13) and (15) can be substituted into (23) and (24), respectively. It follows

$$\underline{B}_{2,0} \approx -\frac{2}{\sqrt{5}}\underline{B}_{0,0} \tag{25}$$

and a normalization yields the transversal dependence of the secondary wave

$$\underline{D}_{\mathrm{D}}(\Theta,\Phi) \sim \underline{Y}_0^0(\Theta,\Phi) + \frac{2}{\sqrt{5}}\underline{Y}_2^0(\Theta,\Phi)\ . \tag{26}$$

The secondary directivity pattern obtained by equation (26) is depicted by '▬' in Fig. 3. Additionally, the primary directivity pattern of the dipole source and the squared primary directivity are depicted by '▬' and '▬', respectively. It can be seen that the directivity pattern of the secondary wave equals the squared directivity pattern of the primary wave. Regarding the equations (20) and (21), the squared directivity pattern of the primary wave corresponds to the transversal dependence of the virtual source strength density.

If primary nearfield contributions cannot be neglected, the integrals of (23) and (24) have to be analysed in detail. For this purpose, the relations for the spherical Bessel functions [8]

$$j_2(k_{\mathrm{d}}r) = -j_0(k_{\mathrm{d}}r) - 3\frac{\cos(k_{\mathrm{d}}r)}{k_{\mathrm{d}}^2r^2} + 3\frac{\sin(k_{\mathrm{d}}r)}{k_{\mathrm{d}}^3r^3}\ , \tag{27}$$

and for the spherical Hankel functions

$$\underline{h}_2(kr) = -\underline{h}_0(kr) - 3\frac{e^{\mathrm{j}k_{\mathrm{d}}r}}{k_{\mathrm{d}}^2r^2} - 3\frac{e^{\mathrm{j}k_{\mathrm{d}}r}}{k_{\mathrm{d}}^3r^3} \tag{28}$$

can be used to simplify the calculations. Without stating the analytical solution in detail, generic secondary directivity patterns obtained by equation (23) are shown in Fig. 3 depicted by the grey lines. The parametrizations are chosen according to an in air parametric communication system reported in [7], e.g., α=0,01/m, $k_{1,2}$=(760 ± 10) /m and c_0 = 330 m/s. To vary the contribution of the primary nearfield, the integration in (23) and (24) was evaluated for different lower bounds $r = r_0$. For the upper bound, the limit $r \to \infty$ was determined.

With r_0=2/k_{d}=10 cm, depicted by '▬' in Fig. 3, the secondary directivity is in a good agreement to the directivity obtained by using the approximation (26), depicted by '▬' in Fig. 3. Setting r_0=1/k_{d}=5 cm, depicted by '▬' in Fig. 3, the influence of the primary nearfield can be mainly seen far-off the acoustical axis. This is further illustrated by setting r_0=1/2k_{d}=2,5 cm, depicted by '▬' in Fig. 3. As a result, a widening of the directivity pattern is caused by the primary nearfield.

Summary

This paper shows that a spherical harmonic expansion of both the primary wave and the Green's function simplifies the study of the nonlinearly generated secondary wave. This way, closed form solutions can be found by separating the volume integral in a radial and a transversal dependent component.

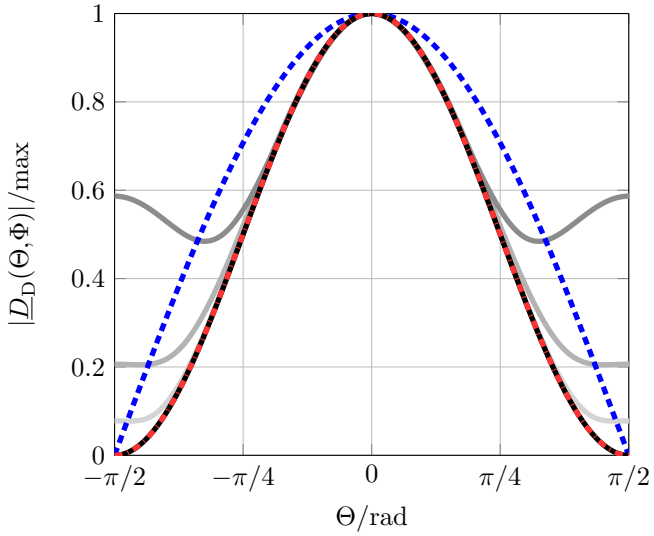

Fig. 3: Directivity analysis of a dipole source: Primary directivity pattern ('▬') and squared primary directivity pattern ('▬'); Secondary directivity pattern ('▬') obtained by the approximation of (26); Secondary directivity patterns considering primary nearfield contributions with r_0=2/k_{d} ('▬'), r_0=1/k_{d} ('▬') and r_0=1/2k_{d} ('▬').

As an example, the secondary directivity of a z-axial dipole source is studied. Considering only primary farfield contributions, the secondary directivity is determined without explicitly solving the volume integration. It is shown that the secondary directivity caused by the primary farfield approaches the squared directivity of the primary wave. It is further shown that primary nearfield contributions result in a broadening of the secondary directivity pattern.

Bibliography

[1] K. Wiedmann, T. Buch, and T. Weber, "Parametric underwater communications," *Proc. 11th European Conference on Underwater Acoustics (ECUA12)*, pp. 1378–1385, Edinburgh, 2012.

[2] M. B. Moffett and R. H. Mellen, "Model for parametric acoustic sources," *Journal of the Acoustical Society of America*, vol. 61, no. 2, pp. 325–337, 1977.

[3] R.F.W. Coates, M. Zheng, and L. Wang, "BASS 300 PARACOM: A model underwater parametric communication system," *IEEE Journal of Oceanic Engineering*, vol. 21, no. 2, pp. 225–232, 1996.

[4] L. Kopp, D. Cano, E. Dubois, L. Wang, B. Smith, and R. F. W. Coates, "Potential performance of parametric communications," *IEEE Journal of Oceanic Engineering*, vol. 25, no. 3, pp. 282–295, 2000.

[5] P. J. Westervelt, "Parametric acoustic array," *Journal of the Acoustical Society of America*, vol. 35, no. 4, pp. 535–537, 1963.

[6] Earl G. Williams, *Fourier Acoustics: Sound Radiation and Nearfield Acoustical Holography*, Academic Press, 1999.

[7] K. Wiedmann and T. Weber, "A grey-box modelling approach for the nonlinear parametric channel.," *IEEE International Conference on Acoustics, Speech, and Signal Processing (ICASSP'14)*, pp. 4327–4331, Florence, 2014.

[8] Milton Abramowitz and Irene A. Stegun, *Handbook of Mathematical Functions*, Dover Publications, New York, 1965.